

# *Gaia*-Sausage-Enceladus: Lithium evolution from early red-giant-branch and main-sequence stars

C. T. Nguyen<sup>1,2</sup> \*, G. Cescutti<sup>1,2</sup>, M. M. Bennedik<sup>3</sup>, P. Molaro<sup>2</sup>, L. Magrini<sup>4</sup>, and A. J. Korn<sup>5</sup>

<sup>1</sup> Department of Physics, University of Trieste, Piazzale Europa, 1, Trieste, Italy

<sup>2</sup> INAF-Osservatorio Astronomico di Trieste, Via Giambattista Tiepolo, 11, Trieste, Italy

<sup>3</sup> Institut für Astronomie und Astrophysik, Eberhard Karls Universität Tübingen, Sand 1, 72076 Tübingen, Germany

<sup>4</sup> INAF, Osservatorio Astrofisico di Arcetri, Largo E. Fermi 5, 50125 Firenze, Italy

<sup>5</sup> Department of Physics and Astronomy, Uppsala University, Box 516, SE-75120 Uppsala, Sweden

## ABSTRACT

The combination of data from the *Gaia* satellite and large ground-based spectroscopic surveys recently lead to a milestone understanding of our Galaxy's formation history, marked by the identification of stellar remnants of the accreted *Gaia*-Sausage-Enceladus (GSE) dwarf galaxy. Lithium (Li) remains one of the most difficult elements to explain because of its complex behaviour over evolutionary timescales: both the Spite plateau observed in metal-poor main-sequence (MS) stars and the recently discovered Li plateau of early red-giant-branch (eRGB) stars in the Milky Way challenge current galactic chemical evolution models. In this article, we investigate the viability of these Li-plateau features in the GSE galaxy, using public data from current big surveys: GALAH, *Gaia*-ESO, and the collective SAGA database. We present a chemical evolution model of Li for GSE and find agreement with the observed data. We find the signature of Li plateau at low metallicities in both eRGB and MS stars. At higher metallicities, we see candidates of the Li-enriched stars that have their main contribution from nova explosions. These results reinforce the universality of the Spite plateau, and indicate that the eRGB Li plateau might also be a universal feature across different galactic systems. A hint of low nova Li yield in GSE is suggested by our eRGB sample from GALAH. However, the lack of stars at high metallicities, possibly caused by the merger event, prevents a precise study of nova contributions, and we expect that upcoming data will enable a more comprehensive analysis.

**Key words.** Stars: abundances - Galaxies: abundances - Galaxies: evolution

## 1. Introduction

Mergers with nearby galaxies have affected the structure and formation of the Milky Way (MW), which is formed via two main processes: in-situ formation and accretion. While in-situ stars were formed within the main body of the MW, accreted stars originated from nearby galaxies and were incorporated into it over time (Deason et al. 2016). The most prominent event is the major merger of the *Gaia*-Sausage-Enceladus (GSE) dwarf galaxy occurred roughly 10 Gyr ago (Helmi et al. 2018). Thanks to the astrometric data from *Gaia* (Gaia Collaboration et al. 2016) and the spectroscopic survey Apache Point Observatory Galactic Evolution Experiment (APOGEE; Majewski et al. 2017), the identification of substructures in the MW stellar halo led to a profound discovery of the GSE stellar populations (Helmi et al. 2018; Belokurov et al. 2018; Myeong et al. 2019). This merger event perturbed the formation and evolution of the MW (Carrillo et al. 2026). Hence, it is crucial to understand the formation history of GSE progenitor. Historically, Nissen & Schuster (2010) was the first to identify two distinct halo populations with high- and low- $[\alpha/\text{Fe}]$  sequences, of which the lower  $[\alpha/\text{Fe}]$  sequence was argued to be an accreted population. This was later confirmed by the discovery of GSE. Since then, many studies have delved into the reconstruction of GSE star formation history using its stellar abundances (e.g. Vincenzo et al. 2019; Hasselquist et al. 2021). Recently, by comparing the evolution of Mg, Fe, Ba and Eu with that of Sculptor and Fornax galaxies, Erandes et al. (2024) suggested that GSE

underwent a slow gas-enrichment first, then followed by a star formation phase and quenched by the merger. The metallicity range of GSE remnants is usually between  $-3 \leq [\text{Fe}/\text{H}] \leq -0.6$ , with the metallicity distribution function (MDF) peaking at  $[\text{Fe}/\text{H}] \approx -1.2$  (Feuillet et al. 2021; Limberg et al. 2022).

Lithium (Li) is a fragile element, easily destroyed in the stellar interior at  $\sim 2.5 \times 10^6$  K (Pinsonneault 1997). Observations of warm and metal-poor main-sequence (MS) halo stars reveal a Li plateau, known as the Spite plateau (Spite & Spite 1982), with an average abundance of  $A(\text{Li}) \approx 2.2$  dex. In contrast, standard Big Bang Nucleosynthesis predictions (Coc et al. 2014), assuming the cosmological parameters of Planck Collaboration et al. (2014), yield a higher primordial value,  $A(\text{Li}) \approx 2.7$  dex, leading to the well-known 'cosmological Li problem'. Stellar internal processes certainly play a role, as the stars we observe today have evolved over the past 10–12 Gyr (Korn et al. 2007; Fu et al. 2015; Gao et al. 2020). Meanwhile, stars at solar neighbourhood metallicity show a complex pattern of Li enrichment and depletion that may originate from many sources, e.g. cosmic rays (Prantzos 2012), nova explosions (Cescutti & Molaro 2019), stellar mixing processes (Borisov et al. 2024) and intrinsic properties (Dantas et al. 2025). These features make Li one of the most interesting elements to study galactic chemical evolution (see Charbonnel & Prantzos 2026, for a thorough review).

Recent study by Nguyen et al. (2025b, hereafter Paper I) implemented corrections from stellar evolution as a possible explanation to the cosmological Li problem, and for the first time used early red-giant-branch (eRGB) stars to study Galactic Li evolution. Accordingly, chemical evolution model traces the evolution

\* Corresponding author: chi.nguyen@inaf.it

of an element in the interstellar medium. For Li, which is easily destroyed during the evolution of stars, a correction due to stellar evolution is thus embedded into the model to reproduce the abundances observed in stars at different evolutionary phases.

Moreover, literature has confirmed the universality of the Spite plateau observed in MS stars in different galactic systems (e.g. Monaco et al. 2010; Nissen & Schuster 2012; Molaro et al. 2020a; Simpson et al. 2021). In this article, we first investigate the presence of the eRGB Li plateau in the GSE, and second present a galactic chemical evolution model for Li of the GSE. We adopt the available data from the Galactic Archaeology with HERMES survey (GALAH, De Silva et al. 2015), complemented by data from the SAGA database (Suda et al. 2008) and the *Gaia*-ESO survey (Gilmore et al. 2012). Details of the selection method for GSE members are described in Sect. 2. In Sect. 3, we present a chemical evolution model for GSE. The obtained results are shown in Sect. 4, and we conclude this paper in Sect. 5.

## 2. Sample selection and kinematics

To study the Li evolution of GSE, we use data from the three catalogues GALAH DR3 (Wang et al. 2024), SAGA (Suda et al. 2008) and *Gaia*-ESO (Magrini et al. 2021). We select the GSE members using the kinematic selection criteria defined by Feuillet et al. (2021), i.e. an angular momentum perpendicular to the galactic plane of  $-500 \leq L_z$  (kpc km s<sup>-1</sup>)  $\leq 500$ , and a radial action of  $30 \leq \sqrt{J_r}$  (kpc km s<sup>-1</sup>)  $\leq 55$  (the so-called  $L_z$ - $J_r$  method).

For stars in the GALAH DR3 catalogue, we adopt the heliocentric coordinates and space velocities from Buder et al. (2021). For stars in the SAGA and *Gaia*-ESO catalogues, these values are not provided and have to be computed. First, we seek the astrometric parameters from the *Gaia* DR3 catalogue (Gaia Collaboration et al. 2023) by query at CDS using the star identification included in these catalogues. For radial velocities, we adopt the values provided in these catalogues if available, and from *Gaia* DR3 otherwise. Then, we compute the coordinates and space velocities from the astrometric parameters with the transformations outlined in Sect. 4.1.7.1 of Hobbs et al. (2022).

We compute the orbital parameters with the Python package GALPY (Bovy 2015). To be consistent with Feuillet et al. (2021), we use the MWPOTENTIAL2014 package and Stäckel approximation (Binney 2012), adopting the same distance of the Sun to Galactic centre  $R_\odot = 8.0$  kpc (Bovy et al. 2012), its vertical offset to the Galactic plane  $Z_\odot = 25$  pc (Jurić et al. 2008) as well as the space velocities  $(U, V, W)_\odot = (11.1, 12.24, 7.25)$  km/s (Schönrich et al. 2010) with a local standard of rest  $V_{\text{LSR}} = 220$  km/s (Bovy et al. 2012). Using the kinematic  $L_z$ - $J_r$  selection method, we obtain 1257 stars from the GALAH DR3 catalogue (with high data quality: `flag_fe_h=0` and `flag_sp=0`), 32 stars from SAGA and 8 stars from *Gaia*-ESO that belong to the GSE system. The stellar parameters, Li abundance and kinematic properties of these stars are listed in Tables A.1 and A.2.

We further select the samples of MS and eRGB stars by applying conditions to  $T_{\text{eff}}$  and  $\log g$ . In particular, we select stars within  $5800 \leq T_{\text{eff}}$  (K)  $\leq 6900$  and  $3.8 \leq \log g$  (cm s<sup>-2</sup>)  $\leq 4.5$  for our MS sample. For the eRGB stars, we define a synthetic line along the RGB phase within a narrow range of  $4800 \leq T_{\text{eff}} \leq 5200$  and  $2.4 \leq \log g \leq 3.3$ . Then, we select stars within the range of  $T_{\text{eff}}^{\text{synthetic}} \pm 200$  K for our eRGB sample. These choices of  $T_{\text{eff}}$  and  $\log g$  are to avoid stars undergoing Li depletion due to convective driven and thermohaline mixing. The Kiel and A(Li) vs.  $\log g$  diagrams of stars in the two samples are shown in Fig. 1.

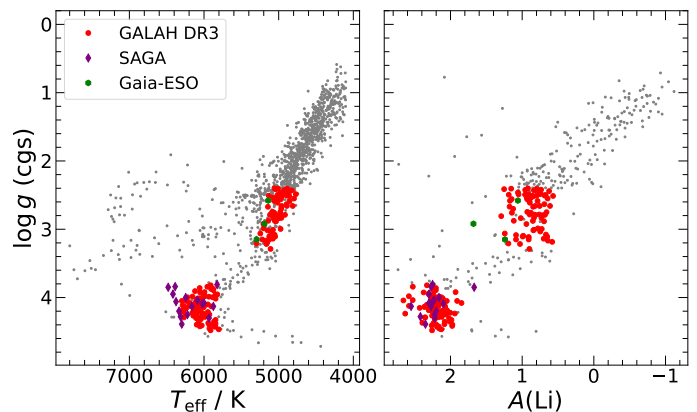


**Fig. 1.** Samples of MS and eRGB stars of GSE from the GALAH, SAGA and *Gaia*-ESO catalogues. Left panel: Kiel diagram. Right panel: Variation of A(Li) along with  $\log g$ . The full sample of GSE from the GALAH catalogue is shown in the background (grey dots).

**Table 1.** Computed values of the six free parameters and their best constrained values.

parameter	range ( $[min, max, step]$ )	best-constraint
$M_{\text{GSE}}$ ( $M_\odot$ pc <sup>-2</sup> )	[1, 3, 0.5]	2.38
$\tau$ (Myr)	[500, 1000, 50]	729
$\sigma$ (Myr)	[1000, 2000, 100]	1569
$\nu_{\text{SFR}}$ (Gyr <sup>-1</sup> )	[0.3, 1.3, 0.1]	1.01
$\nu_{\text{wind}}$	[3, 9, 1]	6.83
$T_{\text{wind}}$ (Myr)	[2100, 3100, 100]	2900

## 3. Chemical evolution model

In this article, we use the concept introduced in our previous work (Paper I), which takes into account corrections to surface Li from stellar evolution, to study the Li evolution of GSE,

$$A(\text{Li}) = A(\text{Li})_{\text{CEM}} + \Delta A(\text{Li})_{\text{SM}}. \quad (1)$$

The second term in Eq. 1,  $\Delta A(\text{Li})_{\text{SM}}$ , is the correction due to stellar evolution. Similar to our previous work (for studying the Li evolution of the MW's thin disc), we adopt the grids of stellar corrections for surface Li from Nguyen et al. (2025a). The correction term is ultimately dependent on metallicity, since we adopt the empirical mass-metallicity relations in Paper I. More details on deriving  $\Delta A(\text{Li})_{\text{SM}}$  can be found in appendix B.

The first term,  $A(\text{Li})_{\text{CEM}}$ , is the prediction from chemical evolution model. In this article, we adopt an infall model and assume a Gaussian infall rate to describe the accreted gas to form the GSE galaxy (Cescutti et al. 2013). The infall rate is given by

$$\dot{G}_{\text{inf}}(t) = M_{\text{GSE}} \frac{e^{-(t-\tau)^2/2\sigma^2}}{\sigma \sqrt{2\pi}}. \quad (2)$$

Here,  $M_{\text{GSE}}$  is the total mass density of gas accreted into GSE,  $\tau$  is the central peak of the infall distribution, and  $\sigma$  is the standard deviation of the infall law. The star formation rate (SFR) follows the Schmidt's law (Schmidt 1959), which is proportional to the surface gas density (see also Portinari & Chiosi 1999),  $\psi(t) = \nu_{\text{SFR}} \Sigma(t)^k$ , if the evolutionary time of the GSE has not yet reached a threshold value, parametrized as  $T_{\text{SFR}}$ . This value is set to the time when the GSE stops forming stars because of the interaction with the MW. As the evolutionary time goes beyond  $T_{\text{SFR}}$ , the SFR of the GSE is set to zero. In the expression above,

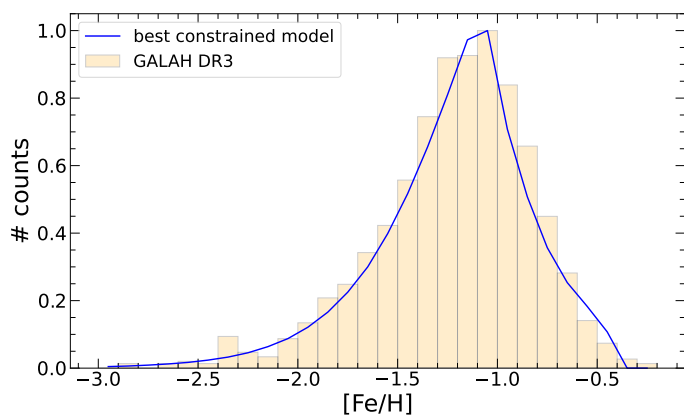


**Fig. 2.** MDF of GSE star members. Data are taken from GALAH DR3, binned in 0.1 dex of  $[\text{Fe}/\text{H}]$ . The displayed model is computed using the best-constrained values of the six parameters in Table 1.

$\nu_{\text{SFR}}$  is the efficiency coefficient of the SFR,  $\Sigma(t)$  is the total surface mass density of gas in GSE, and the exponential coefficient  $k = 1.5$  following Kennicutt (1998). Due to the interaction with the MW, an outflow wind operates for a period of time. In our model, the outflow wind rate is assumed to be proportional to the SFR,  $W(t) = \nu_{\text{wind}}\psi(t)$ , with  $\nu_{\text{wind}}$  as the wind efficiency coefficient. The time when the wind starts is characterised by  $T_{\text{wind}}$ , and before this time the outflow wind rate is set to zero.

In total, our chemical evolution model has seven free parameters:  $M_{\text{GSE}}$ ,  $\tau$ ,  $\sigma$ ,  $\nu_{\text{SFR}}$ ,  $T_{\text{SFR}}$ ,  $\nu_{\text{wind}}$  and  $T_{\text{wind}}$ . The first calibration of these parameters was done in Cescutti et al. (2020) using the APOGEE data. In this article, we recalibrate these parameters using GALAH DR3 data. We stress that, in order to reduce the number of free parameters, we assume that GSE stopped forming stars at  $T_{\text{SFR}} \sim 7$  Gyr ago. We then compute several models with given values of the other six parameters and rely on the metallicity distribution function (MDF) to search for the best-fit values. In particular, the parameter space of these six parameters are summarised in Table 1. The normalised  $\chi^2$  method is used to find the best match to the observed MDF. We collect the fits with  $\chi^2 \leq 1$  as our best-match models, and compute the mean values from the obtained results for each parameters. The best constrained values are listed in Table 1. The MDF predicted by our model, computed with the best constrained values, is shown in Fig. 2 and superimposed on the observed MDF of GSE. Moreover, we assume the ISM's Li abundance is the cosmological value ( $A(\text{Li}) = 2.69$  dex; Coc et al. 2014) in our calculations.

Furthermore, Li enrichment in the solar vicinity is explained by the contribution of Li produced by novae. We adopt the prescription of Cescutti & Molaro (2019) to take into account their contribution. Here, we adopt the delay time between when the primary star became a white dwarf and the nova explosion takes place,  $\tau_{\text{nova}} = 1$  Gyr; we also adopt a mean nova Li yield,  ${}^{\text{Li}}Y_{\text{nova}} = 2.02 \times 10^{-5} M_{\odot}$ , that is computed from observational data of Li production per nova event in the literature (Tajitsu et al. 2015; Molaro et al. 2016; Tajitsu et al. 2016; Izzo et al. 2018; Molaro et al. 2020b; Arai et al. 2021; Molaro et al. 2022, 2023; Izzo et al. 2025). We should clarify that an assumption that all novae produce the same amount of Li in all events is adopted in our model, together with a typical number of  $10^4$  outburst events over their entire lifetime (Ford 1978). A computed model without any stellar Li depletion is shown by the pink line in Fig. 3 for later comparisons.

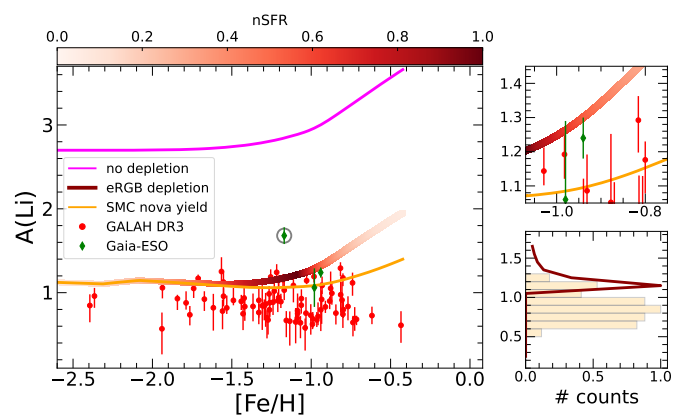


**Fig. 3.** Left-panel: Li evolution of the eRGB stars. Model with Li depletion and  ${}^{\text{Li}}Y_{\text{nova}} = 2.02 \times 10^{-5} M_{\odot}$  is colour-coded by the normalised SFR, while model with  ${}^{\text{Li}}Y_{\text{nova}} = 3.7 \times 10^{-6} M_{\odot}$  is shown by the orange line. A possibly outlier star is circled in grey. Upper-right panel: zoom-in to the region of  $-1.05 \leq [\text{Fe}/\text{H}] \leq -0.75$  of the left panel. Bottom-right panel: stellar distribution in Li abundance.

## 4. Results and discussion

After constraining the free parameters using the MDF, we compute the chemical evolution model for Li assuming the original  $A(\text{Li}) = 2.69$  dex and apply the correction term to take into account the Li depletion. Additional processes such as rotational mixing and angular momentum transport are expected to further enhance the Li depletion (Eggenberger et al. 2022), and intrinsic stellar properties may also contribute to the observed scatter (Dantas et al. 2025). As these effects are currently not included in the stellar correction term, our models preferentially trace the upper envelope of the evolutionary trend, explaining a small but systematic offset in the stellar distribution (Fig. 3, bottom panel).

In Fig. 3 (left panel), we show the 82 eRGB stars of GSE selected from the GALAH DR3 catalogue. It reveals a Li plateau at low metallicities,  $[\text{Fe}/\text{H}] \leq -1.2$ , with a mean value of  $A(\text{Li}) = 0.914$  dex and a standard deviation of 0.15 dex, which is overlapping with the previous finding of Mucciarelli et al. (2022). The Mucciarelli et al. (2022) Li plateau was discovered among 58 field halo eRGB stars with high-resolution spectra, and was reproduced by a Galactic thin disc chemical evolution model in Paper I. In this work, our model including the depletion correction up to the RGB bump is shown as the line coloured by the normalised SFR, indicating a Li-plateau feature at this metallicity range, with an average  $A(\text{Li}) \approx 1.1$  dex. It is in agreement with the upper end of Li data from the GALAH sample. The predicted value is also well consistent with the result of Paper I and the observed plateau in Mucciarelli et al. (2022). This result implies that the eRGB Li plateau may also be a universal feature across different galactic systems.

Novae are thought to play a dominant role in explaining the Li enrichment in the solar vicinity (e.g. Cescutti & Molaro 2019; Kemp et al. 2024). However, after the major merger event with the MW, GSE eventually stopped forming stars at a time possibly  $T_{\text{SFR}} \approx 7$  Gyr ago as we assumed in this work. This prevents the formation of younger stars that are potentially enriched in Li by the former nova explosions. As a result, the amount of GSE stars found in the solar neighbourhood are fewer towards higher metallicities, preventing us from having a better constraint on the nova Li yield. Regardless, we compute our model with an average Li yield of  ${}^{\text{Li}}Y_{\text{nova}} = 2.02 \times 10^{-5} M_{\odot}$  as constrained from the novae observations. Among the GALAH

catalogue, at  $[\text{Fe}/\text{H}] > -1.05$  region, we find that three most Li rich stars are aligning with prediction of our model (see Fig. 3, upper-right panel). Two of these stars, with  $[\text{Fe}/\text{H}] \sim -1$ , are located at the rising base of the enrichment evolution. The other star,  $[\text{Fe}/\text{H}] \approx -0.8$ , lies below our model prediction with an offset of  $\sim 0.07$  dex (including the observed uncertainty). We also show in Fig. 3 three eRGB stars obtained from the *Gaia*-ESO catalogue. Two of these stars show their abundances at the rising base of the enrichment evolution. The other star shows a relatively high Li abundance in comparison with other star members, marked by the grey circle. It has  $A(\text{Li})=1.68$  dex, about 0.6 dex higher than the value reported by Mucciarelli et al. (2022). We notice that its radial action,  $\sqrt{J_R} = 30.08$  ( $\text{kpc km s}^{-1}$ )<sup>1/2</sup>, lies at the border of our selection criterion. This rises question about its membership. Moreover, the existence of Li-rich giants (e.g. Smiljanic et al. 2018) further complicates the interpretation of its nature. We therefore consider it an outlier in this paper. The agreement between our model predictions and the Li abundances of these stars may help constrain the nova Li yield in GSE. However, they are mostly at the rising base of the enrichment evolution, preventing a firm conclusion on the adopted yield.

In addition, within the GALAH sample, a relatively flat trend can be depicted in our eRGB stars. This may suggest that GSE exhibits a lower nova Li yield. We include a model adopting the observed Li production per nova event of the Small Magellanic Cloud (SMC; Izzo et al. 2022), yielding  ${}^{\text{Li}}Y_{\text{nova}} = 3.7 \times 10^{-6} M_{\odot}$ , in Fig. 3 (orange line). The MDF of SMC peaks at  $[\text{Fe}/\text{H}] \sim -1$  (Mucciarelli et al. 2023), which is similar to the GSE metallicity. Our model with low nova Li yield tends to reproduce the flat tendency in eRGB stars, but is quite low to reproduce the most Li rich stars. We should stress that nova Li yield depends on stellar mass and metallicity, and that more work is needed to capture the full complexity of chemical enrichment from a population of novae, particularly for GSE, where stars at higher metallicities are lacking (see Kemp et al. 2022, for more discussion).

The Spite plateau found in the MW had been suggested as a common feature also in other galaxies (e.g. Monaco et al. 2010). Likewise, Molaro et al. (2020a) (hereafter, MCF20) drew a similar conclusion on GSE by adopting data from the GALAH DR2 and SAGA catalogues, aligning with the conclusions of Nissen & Schuster (2012). However, MCF20 determined the GSE members by cross-matching with the former determination of Helmi et al. (2018). In this regard, we recall that we use the new definition of Feuillet et al. (2021) to determine the memberships of GSE (Sect. 2). Due to differences in the definition, we find only 15 stars in our SAGA sample present in the MCF20 sample. Regardless of this limited overlap, we find agreement with MCF20 on the Spite plateau in GSE. In particular, at  $[\text{Fe}/\text{H}] < -1.4$ , our model shows an excellent fit to the observed data, especially of SAGA (Fig. 4, left panel), with a predicted  $A(\text{Li}) \approx 2.14 - 2.31$  dex. Our data at this metallicity range from the GALAH sample indicates a mean Li abundance of  $A(\text{Li}) = 2.2$  dex and a standard deviation of 0.14 dex. Furthermore, Simpson et al. (2021) applied the same GSE selection method to the GALAH DR3 data (Buder et al. 2021) and found that GSE indeed exhibits the same Li plateau ( $A(\text{Li}) = 2.35 \pm 0.12$  dex) as other accreted and in-situ MW stars. This result and the agreement with other studies once again reinforces the universality hypothesis of the Spite plateau across different galactic systems (see also Matteucci et al. 2021).

Similarly to the case of eRGB stars, we could not fully study the contribution of novae at the enrichment evolution by using MS stars. We find only two stars at  $[\text{Fe}/\text{H}] \sim -1$ , each from one catalogue, located at the rising base of the enrichment branch.

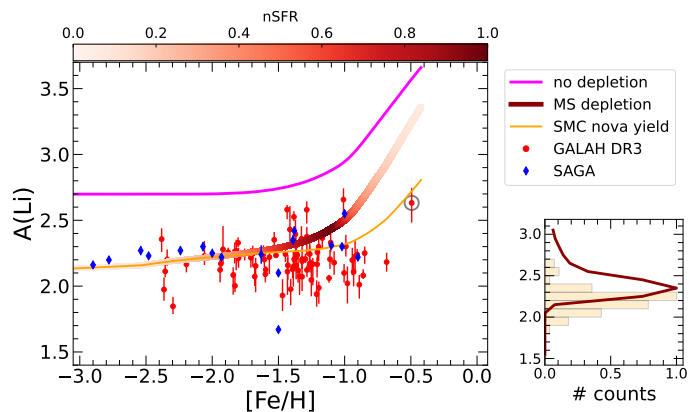


Fig. 4. Same as Fig. 3 but for the MS stars.

Nonetheless, our model, adopting the mean value of observed nova Li yields, predicts the abundances of these two stars very well. The most metal rich star from the GALAH sample in Fig. 4 shows a Li abundance that can be reproduced by lowering the nova Li yield, as indicated by our model with a yield of the SMC. However, radial action of this star,  $\sqrt{J_r} = 30.3$  ( $\text{kpc km s}^{-1}$ )<sup>1/2</sup>, raises questions about its membership. Therefore, we do not rely on this star in our current calibration. In this regard, we note that current and ongoing large surveys are rapidly improving both in data precision and sample sizes. We thus remain optimistic about more robust studies in the future.

Additionally, we should clarify that the GALAH DR4 catalogue (Buder et al. 2025) recently releases a larger sample of stars. However, the catalogue has a problem in the flagging of  $[\text{Fe}/\text{H}]$ , so we cannot select stars with a good determination of iron abundances. For this reason, we chose to adopt data from the GALAH DR3 catalogue in this work. A tentative test using GALAH DR4 data can be found in appendix C. In general, we see similar trends in the  $A(\text{Li})$  versus  $[\text{Fe}/\text{H}]$  diagram between the two catalogues.

## 5. Summary and conclusions

The CEM of Li in a dwarf galaxy is expected to be different from that of the MW. In this context, the accreted GSE stars offer a unique opportunity to study Li evolution in a dwarf galaxy, since dwarf galaxies are often distant and their stellar Li abundances are difficult to measure. We adopt the available data from recent and current big surveys: GALAH DR3, *Gaia*-ESO, and the SAGA database; and use the  $L_z$ - $J_r$  method to determine GSE membership. We then present the Li evolution models for GSE and compare them with the observed data to study the Li plateaus in the MS and eRGB phases. The results reinforce the universality of the Spite plateau and suggest that the eRGB Li plateau may also be universal across different galactic systems. This opens a new category of observational targets for galactic Li evolution studies, since eRGB stars are significantly brighter and easier to observe at high resolution than near-MS stars. Our model also leads to a hint that GSE may exhibit a low nova Li yield, and that improvements in both the modelling of nova contributions and data sample would help to draw more robust conclusions on this matter. To conclude this article, we present in Tables A.1 and A.2 the stellar parameters and kinematic information of GSE stars determined in this paper, available at a Zenodo repository<sup>1</sup>.

<sup>1</sup> <https://doi.org/10.5281/zenodo.19736686>

**Acknowledgements.** We are grateful for the kind and constructive comments and suggestions from the referee, especially on the discussion of nova Li yield. This certainly strengthens our paper. CTN, GC, LM acknowledge the financial support under the National Recovery and Resilience Plan (NRRP), Mission 4, Component 2, Investment 1.1, Call for tender No. 104 published on 2.2.2022 by the Italian Ministry of University and Research (MUR), funded by the European Union – NextGenerationEU – Project ‘Cosmic POT’ (PI: L. Magrini) Grant Assignment Decree No. 2022X4TM3H by the Italian Ministry of Ministry of University and Research (MUR). CTN, GC, AK acknowledge funding from the European Union’s Horizon 2020 research and innovation programme under grant agreement No 101008324 (ChETEC-INFRA). CTN, GC acknowledge the support by INAF Mini grant 2024, ‘‘GALOMS – Galactic Archaeology for Low Mass Stars’’ (1.05.24.07.02). AJK acknowledges support by the Swedish National Space Agency (SNSA). The authors gratefully acknowledge the works behind the *Gaia* mission, ground-based spectroscopic surveys: GALAH, *Gaia*-ESO, and the collective SAGA database, for providing the data used in this work. This work also makes use of the TOPCAT software (Taylor 2005). CTN thanks Emanuele Spitoni, Alexandro Saro, Emma Dodd, Ella Xi Wang, Linda Lombardo and Umberto Maio for helpful discussions over the course of this work.

## References

- Arai, A., Tajitsu, A., Kawakita, H., & Shinnaka, Y. 2021, *ApJ*, 916, 44  
 Asplund, M., Lambert, D. L., Nissen, P. E., Primas, F., & Smith, V. V. 2006, *ApJ*, 644, 229  
 Belokurov, V., Erkal, D., Evans, N. W., Koposov, S. E., & Deason, A. J. 2018, *MNRAS*, 478, 611  
 Binney, J. 2012, *MNRAS*, 426, 1324  
 Boesgaard, A. M. 2007, *ApJ*, 667, 1196  
 Bonifacio, P. & Molaro, P. 1997, *MNRAS*, 285, 847  
 Bonifacio, P., Sbordone, L., Caffau, E., et al. 2012, *A&A*, 542, A87  
 Borisov, S., Charbonnel, C., Prantzos, N., Dumont, T., & Palacios, A. 2024, *A&A*, 690, A245  
 Bovy, J. 2015, *The Astrophysical Journal Supplement Series*, 216, 29  
 Bovy, J., Allende Prieto, C., Beers, T. C., et al. 2012, *ApJ*, 759, 131  
 Buder, S., Kos, J., Wang, X. E., et al. 2025, *PASA*, 42, e051  
 Buder, S., Sharma, S., Kos, J., et al. 2021, *MNRAS*, 506, 150  
 Carrillo, A., Deason, A. J., Fattahi, A., Grand, R. J. J., & Fragkoudi, F. 2026, *MNRAS*, 546, stag111  
 Cescutti, G., Chiappini, C., Hirschi, R., Meynet, G., & Frischknecht, U. 2013, *A&A*, 553, A51  
 Cescutti, G. & Molaro, P. 2019, *MNRAS*, 482, 4372  
 Cescutti, G., Molaro, P., & Fu, X. 2020, *Mem. Soc. Astron. Italiana*, 91, 153  
 Charbonnel, C. & Prantzos, N. 2026, *arXiv e-prints*, arXiv:2602.17470  
 Coc, A., Uzan, J.-P., & Vangioni, E. 2014, *JCAP*, 2014, 050  
 Dantas, M. L. L., Smiljanic, R., Romano, D., et al. 2025, *A&A*, 699, A173  
 De Silva, G. M., Freeman, K. C., Bland-Hawthorn, J., et al. 2015, *MNRAS*, 449, 2604  
 Deason, A. J., Mao, Y.-Y., & Wechsler, R. H. 2016, *ApJ*, 821, 5  
 Eggenberger, P., Buldgen, G., Salmon, S. J. A. J., et al. 2022, *Nat. Astron.*, 6, 788  
 Fernandes, H., Feuillet, D., Feltzing, S., & Skúladóttir, Á. 2024, *A&A*, 691, A333  
 Feuillet, D. K., Sahlholdt, C. L., Feltzing, S., & Casagrande, L. 2021, *MNRAS*, 508, 1489  
 Ford, H. C. 1978, *ApJ*, 219, 595  
 Fu, X., Bressan, A., Molaro, P., & Marigo, P. 2015, *MNRAS*, 452, 3256  
 Gaia Collaboration, Prusti, T., de Bruijne, J. H. J., et al. 2016, *A&A*, 595, A1  
 Gaia Collaboration, Vallenari, A., Brown, A. G. A., et al. 2023, *A&A*, 674, A1  
 Gao, X., Lind, K., Amarsi, A. M., et al. 2020, *MNRAS*, 497, L30  
 Gilmore, G., Randich, S., Asplund, M., et al. 2012, *The Messenger*, 147, 25  
 Hansen, C. J., Nordström, B., Bonifacio, P., et al. 2011, *A&A*, 527, A65  
 Hansen, T., Hansen, C. J., Christlieb, N., et al. 2015, *ApJ*, 807, 173  
 Hansen, T., Hansen, C. J., Christlieb, N., et al. 2014, *ApJ*, 787, 162  
 Hasselquist, S., Hayes, C. R., Lian, J., et al. 2021, *ApJ*, 923, 172  
 Helmi, A., Babusiaux, C., Koppelman, H. H., et al. 2018, *Nature*, 563, 85  
 Hobbs, D., Lindgren, L., Bastian, U., et al. 2022, *Gaia DR3 documentation Chapter 4: Astrometric data*  
 Izzo, L., Molaro, P., Bonifacio, P., et al. 2018, *MNRAS*, 478, 1601  
 Izzo, L., Molaro, P., Cescutti, G., et al. 2022, *MNRAS*, 510, 5302  
 Izzo, L., Siebert, T., Jean, P., et al. 2025, *A&A*, 698, A291  
 Jurić, M., Ivezić, Ž., Brooks, A., et al. 2008, *ApJ*, 673, 864  
 Kemp, A. J., Karakas, A. I., Casey, A. R., et al. 2024, *A&A*, 689, A222  
 Kemp, A. J., Karakas, A. I., Casey, A. R., Kobayashi, C., & Izzard, R. G. 2022, *MNRAS*, 509, 1175  
 Kennicutt, Jr., R. C. 1998, *ApJ*, 498, 541  
 Korn, A. J., Grundahl, F., Richard, O., et al. 2007, *ApJ*, 671, 402  
 Li, H., Aoki, W., Matsuno, T., et al. 2018, *ApJ*, 852, L31  
 Limberg, G., Souza, S. O., Pérez-Villegas, A., et al. 2022, *ApJ*, 935, 109  
 Magrini, L., Lagarde, N., Charbonnel, C., et al. 2021, *A&A*, 651, A84  
 Majewski, S. R., Schiavon, R. P., Frinchaboy, P. M., et al. 2017, *AJ*, 154, 94  
 Masseron, T., Johnson, J. A., Lucatello, S., et al. 2012, *ApJ*, 751, 14  
 Matteucci, F., Molero, M., Aguado, D. S., & Romano, D. 2021, *MNRAS*, 505, 200  
 Meléndez, J., Casagrande, L., Ramírez, I., Asplund, M., & Schuster, W. J. 2010, *A&A*, 515, L3  
 Molaro, P., Bonifacio, P., Cupani, G., & Howk, J. C. 2024, *A&A*, 690, A38  
 Molaro, P., Cescutti, G., & Fu, X. 2020a, *MNRAS*, 496, 2902  
 Molaro, P., Izzo, L., Bonifacio, P., et al. 2020b, *MNRAS*, 492, 4975  
 Molaro, P., Izzo, L., D’Odorico, V., et al. 2022, *MNRAS*, 509, 3258  
 Molaro, P., Izzo, L., Mason, E., Bonifacio, P., & Della Valle, M. 2016, *MNRAS*, 463, L117  
 Molaro, P., Izzo, L., Selvelli, P., et al. 2023, *MNRAS*, 518, 2614  
 Monaco, L., Bonifacio, P., Sbordone, L., Villanova, S., & Pancino, E. 2010, *A&A*, 519, L3  
 Mucciarelli, A., Minelli, A., Bellazzini, M., et al. 2023, *A&A*, 671, A124  
 Mucciarelli, A., Monaco, L., Bonifacio, P., et al. 2022, *A&A*, 661, A153  
 Myeong, G. C., Vasiliev, E., Iorio, G., Evans, N. W., & Belokurov, V. 2019, *MNRAS*, 488, 1235  
 Nguyen, C. T., Bressan, A., Korn, A. J., et al. 2025a, *A&A*, 696, A136  
 Nguyen, C. T., Cescutti, G., Matteucci, F., et al. 2025b, *A&A*, 703, A204  
 Nissen, P. E. & Schuster, W. J. 2010, *A&A*, 511, L10  
 Nissen, P. E. & Schuster, W. J. 2012, *A&A*, 543, A28  
 Pinsonneault, M. 1997, *ARA&A*, 35, 557  
 Planck Collaboration, Ade, P. A. R., Aghanim, N., et al. 2014, *A&A*, 571, A16  
 Portinari, L. & Chiosi, C. 1999, *A&A*, 350, 827  
 Prantzos, N. 2012, *A&A*, 542, A67  
 Richard, O., Michaud, G., & Richer, J. 2005, *ApJ*, 619, 538  
 Sakari, C. M., Placco, V. M., Farrell, E. M., et al. 2018, *ApJ*, 868, 110  
 Sbordone, L., Bonifacio, P., Caffau, E., et al. 2010, *A&A*, 522, A26  
 Schmidt, M. 1959, *ApJ*, 129, 243  
 Schönrich, R., Binney, J., & Dehnen, W. 2010, *MNRAS*, 403, 1829  
 Simpson, J. D., Martell, S. L., Buder, S., et al. 2021, *MNRAS*, 507, 43  
 Smiljanic, R., Franciosini, E., Bragaglia, A., et al. 2018, *A&A*, 617, A4  
 Smiljanic, R., Pasquini, L., Bonifacio, P., et al. 2009, *A&A*, 499, 103  
 Spite, M. & Spite, F. 1982, *Nature*, 297, 483  
 Suda, T., Katsuta, Y., Yamada, S., et al. 2008, *PASJ*, 60, 1159  
 Tajitsu, A., Sadakane, K., Naito, H., Arai, A., & Aoki, W. 2015, *Nature*, 518, 381  
 Tajitsu, A., Sadakane, K., Naito, H., et al. 2016, *ApJ*, 818, 191  
 Tan, K. F., Shi, J. R., & Zhao, G. 2009, *MNRAS*, 392, 205  
 Taylor, M. B. 2005, in *Astronomical Society of the Pacific Conference Series*, Vol. 347, *Astronomical Data Analysis Software and Systems XIV*, ed. P. Shopbell, M. Britton, & R. Ebert, 29  
 Vincenzo, F., Spitoni, E., Calura, F., et al. 2019, *MNRAS*, 487, L47  
 Wang, E. X., Nordlander, T., Buder, S., et al. 2024, *MNRAS*, 528, 5394  
 Yang, W., Dou, S., Meng, X., Wu, Y., & Bi, S. 2026, *arXiv e-prints*, arXiv:2602.22516

## Appendix A: Table

Here we present the stellar parameters and Li abundances of 32 stars from the collective SAGA database, along with their references in Table A.1. Meanwhile, for stars from the GALAH (Wang et al. 2024) and Gaia-ESO (Magrini et al. 2021) catalogues, we refer readers to the original catalogues for these properties. In Table A.2, we summarise the kinematic and orbital properties of all GSE stars from three catalogues, determined in this article. These two tables can be found at the mentioned Zenodo repository<sup>1</sup>.

**Table A.1.** Stellar parameters and Li abundances of 32 stars from the SAGA database that belong to the GSE. The last column reports references.

Gaia DR3 ID	Name	$T_{\text{eff}}$ (K)	$\log g$ ( $\text{g cm}^{-2}$ )	A(Li) (dex)	err (dex)	[Fe/H] (dex)	err (dex)	Ref.
4376174445988280576	BD+02_3375	6163	4.13	2.27	0.035	-2.24	—	[1]
1776289248313154688	BD+17_4708	6025	4.09	2.1	0.04	-1.5	0.079	[2]
866863321051682176	BD+24_1676	6387	3.84	2.27	0.035	-2.54	—	[1]
4005317278538492928	BD+26_2251	5875	4.13	2.55	0.05	-1.0	0.079	[2]
1458016709798909952	BD+34_2476	6416	3.95	2.3	0.035	-2.07	—	[1]
761871677268717952	BD+36_2165	6315	4.28	2.42	0.035	-1.38	—	[1]
5762455439477309440	BD-03_2525	5750	3.6	1.96	0.11	-1.8	0.079	[2]
3202470247468181632	BD-06_855	5378	4.43	0.98	0.04	-0.69	0.05	[2]
5510893810476230144	CD-45_3283	5672	4.88	< 0.7	—	-0.83	0.05	[2]
5551565291043498496	CD-48_2445	6222	4.25	2.22	0.01	-1.93	0.05	[3]
5486881507314450816	CD-57_1633	5933	4.3	2.22	0.05	-0.9	0.05	[2]
6573170751851975936	CS22881-039	5950	2.1	< 0.6	—	-2.75	0.19	[4]
6663163201607650688	CS22947-187	5200	1.5	< 0.5	—	-2.61	0.09	[5]
6863245112083068032	CS22950-173	6335	4.2	2.199	0.09	-2.78	0.121	[6]
2676443097097288704	CS22965-054	6245	4.0	2.161	0.09	-2.9	0.136	[6]
2601354871056014336	CS29512-073	5600	3.4	1.93	0.1	-2.14	0.14	[5]
1001659495247619584	G192-43	6298	4.39	2.35	0.035	-1.39	—	[1]
1406910065012679680	G202-65	6480	3.85	1.67	0.04	-1.5	0.16	[7]
2688113962054816128	G26-12	6089	4.04	2.23	0.05	-2.48	0.08	[2]
2502689198705422848	G75-31	6000	4.08	2.3	0.01	-1.02	0.05	[3]
3246885466349457536	HD024289	5700	3.5	2.19	0.08	-2.22	0.1	[7]
615943806835727872	HD084937	6375	4.06	2.25	0.028	-2.0	0.079	[2]
2453397508316944128	HE0134-1519	5500	3.2	1.27	0.19	-3.98	0.3	[8]
4868057499705138560	HE0440-3426	4800	1.6	< 0.26	—	-2.19	0.2	[9]
2988284007989400576	J051727.4-134235	4961	1.93	0.91	0.1	-2.14	0.01	[10]
5602882389229755776	J070520.3-334324	4757	1.27	0.81	0.1	-2.24	0.02	[10]
29184921251610880	LAMOSTJ030209.33+135656.3	5206	2.3	2.34	0.12	-1.74	0.3	[11]
577295698241539840	SDSSJ090733+024608	5934	3.71	2.23	0.1*	-3.42	0.09	[12]
4715919175280799616	CD-61_282	5909	4.59	2.12	0.05	-1.15	0.05	[2]
4272653983123701120	G21-22	5869	3.93	2.24	0.07	-1.63	—	[13]
3510294882898890880	HD111980	5850	3.94	2.31	0.1	-1.1	0.08	[14]
3374633977170787072	HD250792	5568	4.4	1.5	0.035	-1.01	—	[1]

**References.** [1] Meléndez et al. (2010); [2] Smiljanic et al. (2009); [3] Asplund et al. (2006); [4] Hansen et al. (2011); [5] Masseron et al. (2012); [6] Sbordone et al. (2010); [7] Boesgaard (2007); [8] Hansen et al. (2014); [9] Hansen et al. (2015); [10] Sakari et al. (2018); [11] Li et al. (2018); [12] Bonifacio et al. (2012); [13] Bonifacio & Molaro (1997); [14] Tan et al. (2009); \* private communication.

**Table A.2.** Kinematic and orbital parameters of GSE stars in this article. The last four columns are angular momentum in  $z$  direction ( $L_z$ ), total orbit energy ( $E_n$ ), radial action ( $J_r$ ) and vertical action ( $J_z$ ), computed in Sect. 2.

Name	RA (deg)	DEC (deg)	Plx (mas)	...	$L_z$ ( $\text{kpc km s}^{-1}$ )	$E_n$ ( $\text{km}^2 \text{s}^{-2}$ )	$J_r$ ( $\text{kpc km s}^{-1}$ )	$J_z$ ( $\text{kpc km s}^{-1}$ )
SAGA BD+02_3375	264.9383511	2.416891479	9.8386	...	-63.47	-3873.27	2839.32	33.59
SAGA BD+17_4708	332.8830976	18.09309066	7.6143	...	-401.07	-15886.19	1918.38	0.30
⋮	⋮	⋮	⋮	⋮	⋮	⋮	⋮	⋮
GESO J01103865-5008389	17.66100446	-50.14429859	0.3975	...	-160.74	-29247.54	1453.31	90.23
GESO J04392439-4234170	69.85173290	-42.57148078	0.283	...	-293.27	-13440.95	2121.02	144.28
⋮	⋮	⋮	⋮	⋮	⋮	⋮	⋮	⋮
GALAH 131116000501201	51.44879759375034	-68.64119851328851	1.6468	...	-145.62	-18877.52	1841.05	41.21
GALAH 131120002501212	61.66282556896425	-62.03528672946472	0.9815	...	366.32	-24478.15	1480.94	27.07
⋮	⋮	⋮	⋮	⋮	⋮	⋮	⋮	⋮

## Appendix B: The stellar correction term

We here summarise the derivation of  $\Delta A(\text{Li})_{\text{SM}}$  in Eq. 1. The term is computed from grids of stellar tracks, providing the Li depletion from initial value, reflecting Li abundance of the ISM, to a given evolutionary phase (e.g. the MS and eRGB phases).

First of all, it should be recalled that the CEM calculation traces the evolution of a given element in the interstellar medium (ISM; or the stellar birth cloud) across galactic lifetime. Details of CEM for GSE can be found in Sect. 3 of this paper. The Li abundance of ISM, whether cosmological ( $A(\text{Li}) \approx 2.7$  dex) or Spite plateau ( $A(\text{Li}) \approx 2.2$  dex) values, is a debatable subject still to date (see also Molaro et al. 2024). However, in this paper, we assume the Li abundance of ISM is the cosmological value and do not necessarily disown the other scenario, as we showed in Paper I.

For deriving  $\Delta A(\text{Li})_{\text{SM}}$  in the eRGB phase, we adopt the stellar grid of Nguyen et al. (2025a) which includes two sets of tracks of metallicities,  $[\text{Fe}/\text{H}] = -2.4$  and  $-2.1$ , and masses from  $0.65$  to  $0.94 M_{\odot}$ . The predicted stellar-evolution correction is equal to the difference between the initial value in the beginning of the PMS phase and the value when the star reaches the Li-plateau value among RGB stars at a  $\log g$  of  $\sim 2.8$  ( $\text{cm s}^{-2}$ ). We should clarify that these tracks were computed with an initial  $A(\text{Li}) = 2.69$  dex, consistent with the assumed  $A(\text{Li})$  of ISM in our CEM, and subsequently depleted during the PMS phase so that they reach the Spite plateau value at the MS phase. The stellar model prediction was then calibrated to Li data of the globular cluster NGC 6397. Additionally, if the ISM is assumed to have the Spite plateau value, there would be no depletion during the PMS phase as definition. In this case, the predicted stellar-evolution correction is equal to the difference between the value in the MS phase and the value in the RGB phase as defined above. Finally, due to the limited range of metallicity, an extrapolation scheme was applied in case the galactic evolutionary metallicity exceeds the limits of the stellar grid.

A similar approach is applied to derive  $\Delta A(\text{Li})_{\text{SM}}$  in the MS phase. In addition, we must emphasise that there are other mechanisms have been proposed to explain the cosmological Li problem by introducing different stellar extra-mixing prescriptions such as turbulent diffusion (Richard et al. 2005), late mass accretion during the PMS phase (Fu et al. 2015) or rotation and magnetic fields (Yang et al. 2026). Access to these stellar libraries would be valuable for deriving the stellar correction term in our CEM; however, we are at present limited in this regard.

## Appendix C: Analysis using GALAH DR4 data

In this appendix we redo our study in this work by using data from the GALAH DR4 catalogue (Buder et al. 2025). Overall, the sample size increases to 1842 stars, about 500 stars more than the sample using the GALAH DR3 catalogue. Fig. C.1 shows the obtained MDF, indicating an offset with our model prediction, or rather with the GALAH DR3 catalogue. This may be explained by the quality selection in iron abundances, i.e. we cannot select stars with  $\text{flag\_fe\_h}=0$  due to a bug arose in the GALAH DR4. Works in progress to solve this problem and calibrations to further evaluate the new released data have been claimed to be provided in the future (see Buder et al. 2025). Regardless, we then make a tentative analysis on the Li evolution. The results are shown in Figs. C.2 and C.3. For the Li plateaus at low metallicities, we obtain an agreement with our main results in Figs. 3 and 4. The nova Li contribution remains ambiguous.

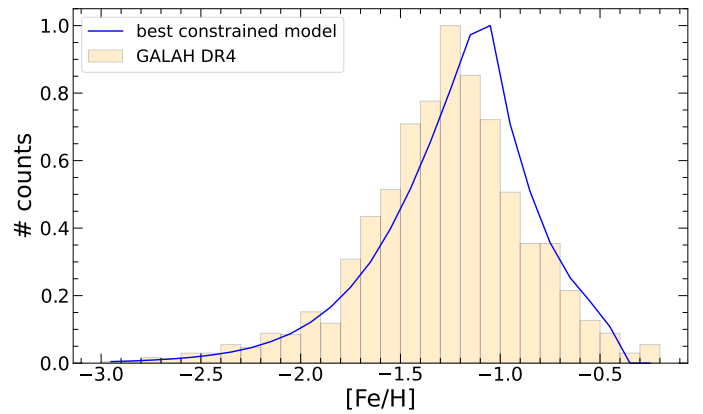


Fig. C.1. MDF of GSE by using the GALAH DR4 data.

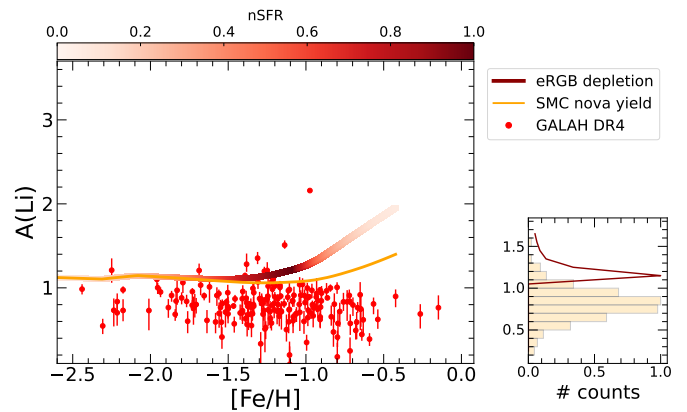


Fig. C.2. Li evolution in eRGB stars by using the GALAH DR4 data.

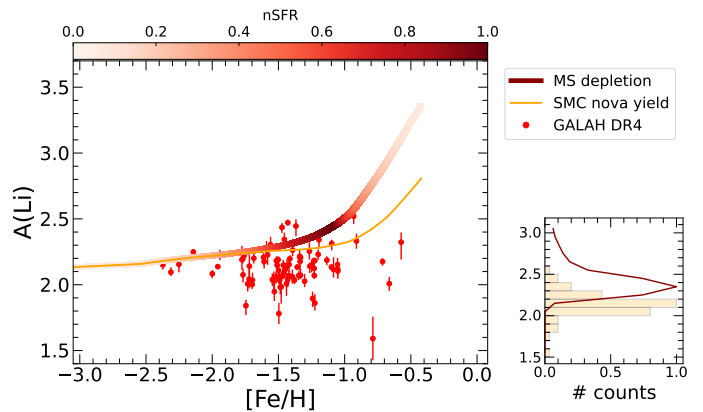


Fig. C.3. Li evolution in MS stars by using the GALAH DR4 data.